# Terahertz transfer onto a telecom optical carrier

S. Dhillon,[a,b] S. Barbieri,[a] C. Sirtori[a]
[a] University Paris VII, 10 rue A. Domont et L. Duquet, 75013 Paris, France.
[b] Ecole Normale Supérieure, 24 rue Lhomond, 75005 Paris, France

**Abstract - Recent progress in the up-conversion of THz signals to the near-infrared region using the second order non-linearity of GaAs is presented. The process is used to demonstrate phase matched intra-cavity THz sideband generation at λ~1.55µm within a THz quantum cascade laser (f=2.8THz). Furthermore, the phase matched point is shown to be tunable over a wide wavelength range via engineering of the THz mode. This up-conversion technique of the QCL emission brings THz signals to the technologically important telecom range.**

## I. Introduction And Background

Considerable advances have been made in the field of terahertz (THz) quantum cascade lasers (QCL) since their first realization in 2002.[1] Within a few years high temperature operation has been achieved and the wavelength range has been extended to 250µm (1.2THz).[2] These sources now cover the technological vacuum between electrical and optical methods to generate radiation. This "THz gap" offers considerable potential applications in astronomy, medical imaging, bio-sensing and free space communications. However, even with these developments in source technology, analyzing these THz signals remains a key issue due to limitations in detector performances (low sensitivity, slow response), and which frequently require cryogenic operation.

In this work, we present and review a scheme that up-converts THz emission to the technologically mature telecom range, permitting new methods to treat these signals. The process is based on a second order non-linear effect and where a THz QCL is used simultaneously as a THz source, waveguide and non-linear medium. The process investigated uses a THz QCL, operating at $\Omega_3$=2.8THz, and an external near-infrared beam, $\omega_1$, from a tunable diode laser which is coupled into a specially designed the QCL cavity. In this configuration the GaAs non-linear susceptibility allows the mixing of the NIR beam with the THz radiation within the QCL, generating sidebands at $\omega_2 = \omega_1 \pm \Omega_3$.

This process is further shown to be phase-matched using the anomalous refractive index dispersion produced by the *restrahlenband*.[3] The wavelengths required for the pump and the THz laser for phase matching can be deduced from the refractive index dispersion of bulk GaAs, shown as a function of wavelength in Fig. 1. Since $\omega_1,\omega_2 >> \Omega_3$, energy and momentum conservation are satisfied when:[9]

$$n_3 = n_1 + \left.\frac{dn(\omega)}{d\omega}\right|_{\omega_1} \left(\omega_1 - \Omega_3\right) \qquad (1)$$

where $n_1$ and $n_3$ are the refractive indices of the NIR and THz waves, respectively. The term on the right hand side of equation (1) is plotted as a red line in Fig. 1. This illustrates the wavelengths involved in the phase-matched process. For example, it is highlighted that, for bulk GaAs, 100µm (3THz) is phase matched to ~1.3µm. Indeed, it is possible to achieve phase-matching from ~6THz down to virtually DC using NIR wavelengths from 1 to 1.4 µm. In bulk material, however, for a given THz frequency $\Omega_3$ there is only one pair $\omega_1$, $\omega_2$ that satisfies condition (1). This crucial constraint is relaxed in this work, since the nonlinear interaction occurs among *guided* waves with very different spatial extensions. Due to the large differences in wavelengths, the refractive index of the NIR mode $n(\omega_1)$ is essentially independent of the waveguide geometry, while the THz index $n(\Omega_3)$ is strongly affected by the laser ridge width; a reduction of the width increases the lateral overlap of the THz guided mode with the air surrounding the laser ridge, thus decreasing its effective refractive index. This modal phase matching technique allows the shift of the phase matched point for $\Omega_3$ = 2.8THz, from the NIR bulk-related value at 1.3µm towards and beyond 1.55µm, i.e. at the transmission peak of optical fibers.[4,5] Fig. 2 shows the phase-matched NIR pump wavelength as a function of the ridge width for a THz laser emitting radiation at 2.8THz (107µm), showing that for a ridge width of 47µm the phase matching point is at 1.56µm.

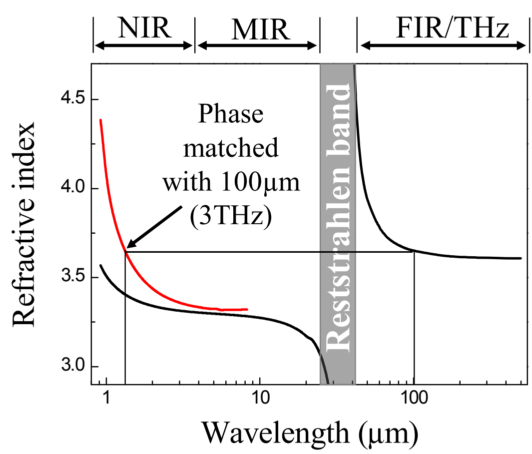


**Fig. 1**. **Principle of phase matching between the NIR and THz ranges**. Refractive index of bulk GaAs as a function of wavelength, illustrating the larger refractive index in the THz range compared to the mid- and near-infrared. The red curve is an approximation of the phase matching condition showing the NIR wavelength required for phase matching for a given THz index (and hence frequency). For example it is shown that 3THz (100µm) with a refractive index of 3.65 is phase matched to ~1.3µm.

This tuning of the phase match point is only possible for a double metal waveguide, where the active region is sandwiched between two metal strips, as the mode is tightly confined between these layers. In the case of single plasmon

978-1-4244-2120-6/08/$25.00 ©IEEE.

devices, a reduction of the ridge width causes the optical mode to leak further into the substrate, preventing an overlap with the air surrounding the ridge which is used to reduce the THz modal index.

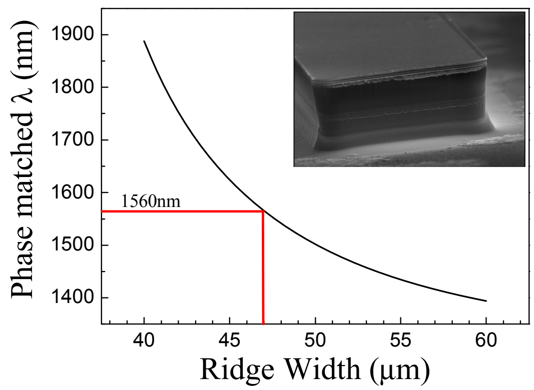


**Fig. 2.** Phase matched wavelength as a function of ridge width showing phase matching at 1560nm with a ridge of width 47μm. Inset: SEM photograph of double metal THz QCL ridge realised using RIE. Almost vertical sidewalls are achieved with good control of the ridge dimensions.

Figure 3 shows the typical fiber coupled spectra obtained for a double metal based waveguide of ridge width 47μm, with the sidebands clearly visible for a pump at 1.56μm. By plotting the ratio between the optical power in one of the sidebands and the injected power (i.e. $P(\omega_2)/P(\omega_1)$) as a function of pump wavelength for four different waveguides, we obtain the data of Fig. 4. Unequivocally, we observe that the phase matching curves shift towards longer wavelengths as the ridge size is decreased, thus demonstrating the control of the non-linear conversion process across the whole telecom range, from 1.3 to 1.6μm. The phase matching point and FWHM of the curve are 1.56μm and 8.5THz, respectively, for the 47μm ridge. The detected conversion efficiency at the phase matching point is $\sim 1\times 10^{-5}$, approximately an order of magnitude smaller than expected due to the high optical losses of the waveguide for the pump and sideband.

This work shows the possibility to transfer THz radiation onto a telecom optical carrier and thus taking advantage of the technology available to this range (sources, detectors, fibre-based devices). Furthermore, we will introduce methods to increase the conversion efficiency by reducing the optical losses and how the technique can be reversed to generate THz radiation. Recent measurements on the utility of this technique to the direct modulation (to 13GHz) of THz QCLs will also be presented.[6]

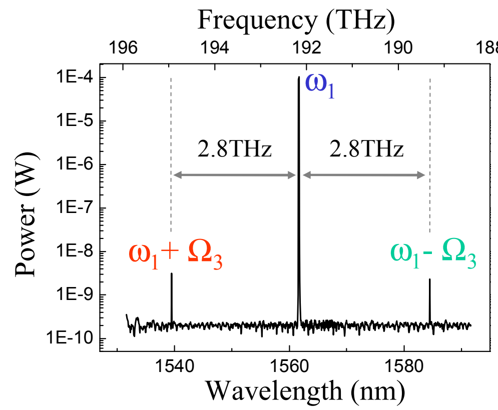


**Fig. 3**. **THz sideband generation in the telecom range.** The sidebands are generated within cavity of THz QCL at $\omega_2 = \omega_1 \pm \Omega_3$ where $\omega_1$ is the NIR pump and $\Omega_3$ is the QCL frequency (2.8THz).

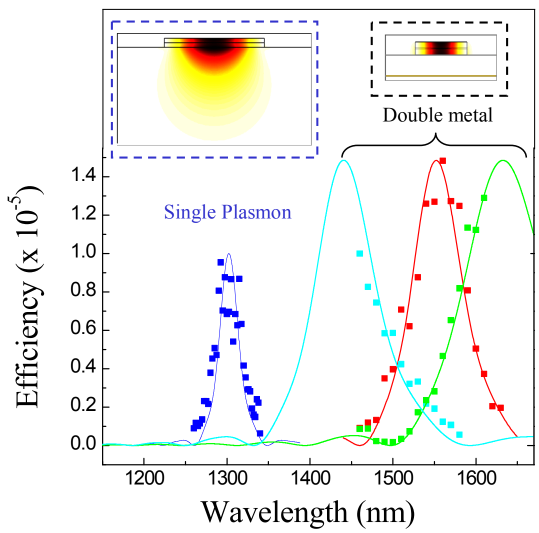


**Fig. 4. Phase match curves of the THz sideband generation for single plasmon and double metal THz QCLs**. The efficiency of the sideband generation as a function of pump wavelength at 10K is shown for two different waveguide geometries. The dark blue curve corresponds to a single plasmon guide and shows phase matching at 1.3μm, close to the bulk related value. The efficiency for a double metal guide for ridge sizes 52μm, 47μm and 42μm are shown in cyan, red and green, respectively, illustrating a shift of the phase matched point towards longer wavelengths. This is a result of a decrease of the THz modal index as the ridge size is reduced. For a ridge size of 47μm, phase matching is achieved at 1.56μm. For clarity, the data plotted are taken at the maximum of the fabry perot oscillations shown in figure 6.

## References


[1] R. Köhler, A. Tredicucci, F. Beltram, H. Beere, E. H. Linfield, A. G. Davies, D. A. Ritchie, R. C. Iotti, and F. Rossi, Nature **417**, 156 (2002).

[2] C. Walther, M. Fischer, G. Scalari, R. Terazzi, N. Hoyler, J. Faist, Appl. Phys. Lett. **91,** 131122 (2007).

[3] V. Berger and C. Sirtori, *Semicond. Sci. Technol.* **19**, 964 - 970 (2004).

[4] S. S. Dhillon, C. Sirtori, A. de Rossi, M. Calligaro, H. E. Beere, S. Barbieri, E. H. Linfield, D. A. Ritchie, *Appl. Phys. Lett.*, 87, 071101 (2005).

[5] S. Dhillon, C. Sirtori, J. Alton, S. Barbieri, A. de Rossi, H. Beere, D. Ritchie, *Nature Photonics* **1**, 426 (2007).

[6] S. Barbieri, W. Maineult, S. S. Dhillon, C. Sirtori, J. Alton, N. Breuil, H. E. Beere, D. A. Ritchie, *Appl. Phys. Lett.* **91**, 143510 (2007).